Cell Reports, Volume *42*

Supplemental information

TGF-β in the microenvironment induces a physiologically occurring immune-suppressive senescent state

Satoru Matsuda, Ajinkya Revandkar, Taronish D. Dubash, Arvind Ravi, Ben S. Wittner, Maoxuan Lin, Robert Morris, Risa Burr, Hongshan Guo, Karsen Seeger, Annamaria Szabolcs, Dante Che, Linda Nieman, Gad A. Getz, David T. Ting, Michael S. Lawrence, Justin Gainor, Daniel A. Haber, and Shyamala Maheswaran

SUPPLEMENTAL TABLES

Table S1: **The full description of the set of leading-edge genes related to the cellular processes shown in Figure 2A, and Figure S3A.**

#	Signatures	GO
1	DNA_REPLICATION_INITIATION	GO:0006270
2	DNA_REPLICATION	GO:0006260
3	CELL_CYCLE_G1_S_PHASE_TRANSITION	GO:0044843
4	CELL_CYCLE	GO:0007049
5	DNA_DEPENDENT_DNA_REPLICATION	GO:0006261
6	DNA_METABOLIC_PROCESS	GO:0006259
7	CELL_CYCLE_PROCESS	GO:0022402
8	CELL_CYCLE_PHASE_TRANSITION	GO:0044770
9	CHROMOSOME	GO:0005694
10	MITOTIC_CELL_CYCLE	GO:0000278
11	CHROMOSOMAL_REGION	GO:0098687
12	CHROMOSOME_ORGANIZATION	GO:0051276

Table S2: Characteristics of NSCLC patients treated with immune checkpoint inhibitors, related to use biological samples in STAR METHODS. See also Figure 5 and S6.

	Patient_Age_at_Diagnosis	Patient_Sex	Initial_Stage	Agent_PD1
Patient 1	58	M	4	Nivolumab
Patient 2	58	F	4	Nivolumab
Patient 3	75	M	3	Nivolumab
Patient 4	52	F	4	Nivolumab
Patient 5	54	M	3	Nivolumab
Patient 6	79	M	1	Nivolumab
Patient 7	75	M	4	Nivolumab
Patient 8	71	M	3	Nivolumab
Patient 9	78	M	3	Nivolumab
Patient 10	73	M	3	Pembrolizumab
Patient 11	71	M	1	Nivolumab
Patient 12	62	M	3	Nivolumab
Patient 13	75	M	3	Atezolizumab
Patient 14	68	M	4	Nivolumab
Patient 15	60	F	4	Nivolumab
Patient 16	66	M	1	Atezolizumab
Patient 17	57	F	3	Nivolumab
Patient 18	75	F	4	Pembrolizumab
Patient 19	78	M	3	Nivolumab
Patient 20	58	F	2	Nivolumab
Patient 21	70	F	4	Pembrolizumab
Patient 22	81	M	1	Nivolumab + Ipilimumab
Patient 23	65	F	1	Nivolumab + Ipilimumab
Patient 24	48	F	2	Nivolumab
Patient 25	64	F	4	Nivolumab
Patient 26	47	F	4	Nivolumab
Patient 27	63	F	4	Nivolumab
Patient 28	52	F	4	Pembrolizumab
Patient 29	50	F	1	Pembrolizumab
Patient 30	64	F	4	Pembrolizumab
Patient 31	80	M	4	Nivolumab + Ipilimumab
Patient 32	78	F	4	Atezolizumab
Patient 33	66	F	4	Pembrolizumab
Patient 34	62	M	3	Nivolumab
Patient 35	57	F	4	Nivolumab + Ipilimumab
Patient 36	79	M	NA	Pembrolizumab

Patient 37	65	M	4	Nivolumab
Patient 38	68	F	4	Pembrolizumab
Patient 39	63	M	4	Atezolizumab
Patient 40	76	F	4	Atezolizumab
Patient 41	68	M	3	Pembrolizumab
Patient 42	62	F	4	Pembrolizumab
Patient 43	55	F	NA	Pembrolizumab
Patient 44	65	F	3	Atezolizumab

Table S3: List of primers used for Real-time PCR reactions, related to oligonucleotides in STAR METHODS. See also Figure 6.

Gene	Forward	Reverse
E2F1	CATCCCAGGAGGTCACTTCTG	GACAACAGCGGTTCTTGCTC
E2F2	CGTCCCTGAGTTCCCAACC	GCGAAGTGTCATACCGAGTCTT
E2F3	AGAAAGCGGTCATCAGTACCT	TGGACTTCGTAGTGCAGCTCT
CCL	GCTGCTTTCAGCATCCAAGTG	CCAGGGACACCGACTACTG
SLC2A1	CAGTTCGGCTATAACACTGGTG	GCCCCCGACAGAGAAGATG
TNFRSF11B	ACCCAGAAACTGGTCATCAGC	CTGCAATACACACACTCATCACT
GREM1	CTGGGGACCCTACTGCCAA	TTTGCACCAATCTCGCTTCAG
CCL5	GCTGCTTTGCCTACCTCTCC	TCGAGTGACAAACACGACTGC
SCG2	GCTAAGGCGTACCGACTTGG	TTCGGCTCCAGAGATGAGGAA
INHBA	TGAGAGGATTTCTGTTGGCAAG	TGACATCGGGTCTCTTCTTCA
INHA	CCTTTTGCTGTTGACCCTACG	AGGCATCTAGGAATAGAGCCTTC
CSF2	GGCCTTGGAAGCATGTAGAGG	GGAGAACTCGTTAGAGACGACTT
IL1A	CGAAGACTACAGTTCTGCCATT	GACGTTTCAGAGGTTCTCAGAG
IL1B	GCAACTGTTCCTGAACTCAACT	ATCTTTTGGGGTCCGTCAACT
CCL2	TTAAAAACCTGGATCGGAACCAA	GCATTAGCTTCAGATTTACGGGT
CMTM3	GCCGAGTCGGGTCTTTCATTC	GAGGAAGTAAACGGCCAACAG
E-cadherin	GGTTTTCTACAGCATCACCG	GCTTCCCCATTTGATGACAC

SUPPLEMENTAL FIGURE LEGENDS

Figure S1. TGFß induces senescence in normoxic and hypoxic cells

(A) Hypoxia-inducible genes are elevated in cells cultured under 4% oxygen. Protein samples from A549 cells grown under normoxia (20% O_2) or hypoxia (4% O_2) were analyzed for the expression of hypoxia inducible genes. Bar graph shows elevated expression of hypoxia inducible targets in hypoxic A549 cells. (n=3 biological replicates); Bar graph shows Mean±SD; Asterisks represent $p<0.001$ by two-tailed unpaired Student's t-test.

(B) ß-gal activity in TGFß-treated normoxic and hypoxic cells increases over time. A549 cells treated with 5 ng/ml TGFß for 0, 3, 9, 15 and 21 days were stained and sorted for ß-gal activity. The bar graph showing the percentage of ß-gal positive cells for each condition and represents Mean±SD for each condition. (n=3 biological replicates). Asterisk represents $p<0.05$ by Mann-Whitney U test.

(C) TGFß increases ß–gal positivity in HepG2 and TE4 cells. The bar graphs show the percentage of ß-gal positive cells for each condition (5 ng/ml TGFß; 15 days) and represent Mean±SD for each condition. (n=3 biological replicates). Asterisk represents $p<0.05$ by Mann-Whitney U test.

(D) TGFß induces the senescence marker, H3K9Me3, in normoxic and hypoxic cells. Upper panel shows H3K9Me3 staining of untreated and TGFß-treated A549 cells grown under hypoxia and normoxia (5ng/ml TGFß; 15 days). Scale bar: 20µm. Lower panel: western blot of H3K9Me3 protein expression in A549 cells treated with TGFß for 0, 3 and 15 days. GAPDH was used as control. Representative data from two biological replicates.

(E) TGFß does not induce apoptosis in normoxic and hypoxic cells. A549 cells grown under normoxia or hypoxia were treated with 5 ng/ml TGFß for 0 and 15 days and stained with an APC conjugated Annexin V antibody followed by FACS. A549 cells treated with docetaxel for 5 hours were used as control (left most bar). Bar graph shows relative intensity of Annexin V determined by FACS. Untreated normoxic and hypoxic cells were used as control. n=3 biological replicates.

(F) p21 expression in ß-gal-low, ß-gal-medium and ß-gal-high populations sorted from A549 cells treated with TGFß (5 ng/ml, 15 days). Untreated cells are shown as controls. Quantification of p21 band intensities is provided below. p21 expression in untreated normoxic cells was set at 1. GAPDH was used as control. Representative data from two biological replicates.

Figure S2. TGFß induces different states of senescence

(A) Multinucleated cells are prevalent in TGFß-treated hypoxic cultures. The ß-gal-high cells collected from TGFß-treated (5 ng/ml, 15 days) hypoxic TE4 cells were stained with DAPI (red) and tubulin (green). Untreated cells were used as control. Photomicrographs of cells under each condition are shown. Right most panel shows higher magnification images of the binucleated and multinucleated cells within the highlighted panel. Scale bars: 50μM (low magnification) and 20μM (high magnification). Representative data from two biological replicates.

(B) Bar graphs show quantification of the binucleated and multinucleated cells in TGFß-treated (5 ng/ml, 15 days) hypoxic TE4 cultures. Untreated cells are shown as controls.

n=3 biological replicates. Mean±SD was calculated from imaging 10 random fields. Asterisk represents $p<0.05$ by two-tailed unpaired Student's t -test.

(C) The ß-gal-high cells collected from TGFß-treated (5 ng/ml, 3 days) hypoxic HepG2 cells were stained with DAPI (red) and tubulin (green). Untreated cells were used as control. Photomicrographs of cells under each condition are shown. Right most panel: higher magnification images of the binucleated and multinucleated cells within the highlighted panels. Scale bars: 50μM (low magnification) and 20μM (high magnification). Representative data from two biological replicates.

(D) Bar graphs show quantification of binucleated and multinucleated cells in TGFß-treated (5 ng/ml,3 days) hypoxic HepG2 cultures. Untreated cells are shown as controls. n=3 biological replicates. Mean±SD was calculated by imaging 10 random fields. Asterisk represents $p<0.05$ by two-tailed unpaired Student's t-test.

(E) Bar graph shows the concentration of TGFß produced by patient-derived lung CAFs *in vitro* as determined using ELISA assays (n=3 biological replicates). The regular RPMI culture medium used to grow CAFs is shown as control.

(F) TGFß from lung cancer patient-derived cancer associate fibroblasts (CAF) induces senescence. A549 cells (mCherry labelled) were cultured with two different lung cancer patient-derived CAFs for 15 days with or without the TGFß inhibitor, SB431542 (2 μM; TGFß-I). mCherry labelled A549 cells alone treated with TGFß (5 ng/ml, 15 days) in the presence and absence of TGFß-I were used as controls. All cultures were maintained under hypoxia (n=3 biological replicates). At the end of the experiment, cells were stained with ß-gal and the tumor cells were sorted based on mCherry-positivity. The bar

graph shows the percentage of (Mean±SD) ß-gal positive and mCherry positive tumor cells. Asterisks represent $p<0.05$ by two-tailed unpaired Student's t-test.

(G) mCherry labelled A549 cells cultured with patient-derived CAFs for 15 days were stained with ß-gal and the tumor cells were sorted based on mCherry-positivity. The ß-gal high population was stained with DAPI, and tubulin and the fraction of multinucleated cells was quantified. mCherry labelled A549 cells alone untreated or treated with TGFß (5ng/ml) for 15 days and similarly analyzed are shown as control. All cultures were maintained under hypoxia (n=3 biological replicates). Bar graph shows the fraction of multinucleated cells (Mean±SD) under each condition. Asterisks represent $p<0.05$ by two-tailed unpaired Student's t test. n=3 biological replicates.

(H) TGFß-treated ß-gal high hypoxic cells are resistant to drug treatment. The ß-gal-low and ß-gal-high populations collected from 5ng/ml TGFß-treated hypoxic and normoxic A549 cells were cultured for a day in the absence of TGFß and treated with increasing concentrations of cisplatin for 72 hours. The graph shows the relative viability of the cells for each condition (y-axis) under different drug concentrations (x-axis). Untreated cells for each condition [TGFß (-)] are shown as controls. Asterisks represent $p<0.05$ by two-tailed unpaired Student's t-test. Representative data from three biological replicates.

Figure S3. Analysis of gene expression differences in E- and D-senescent cells

(A) Analysis of RNA-Seq data from D- and E- senescent cells demonstrates the suppression of gene expression modules representing cell cycle, DNA replication, DNA damage responses and paracrine senescence signatures (Figure 2A). The heatmap displays leading-edge genes relating to each of the processes shown. n=3 biological replicates. The scale bar

represents the differential expression. T-statistic significant gene sets were defined using an FDR threshold of 0.25. The heatmap rows are sorted based on their GSEA enrichment FDR values from most significant (FDR=3.69e-05) to least significant (FDR=0.217).

(B) The dosage of repressor E2Fs does not change in D-sen cells compared with E-sen cells. The expression of the repressor E2Fs, E2F4, E2F5, E2F6 and E2F7, in untreated A549 cells grown under normoxia and hypoxia, E-sen and D-sen cells is shown. n=3 biological replicates. p values for E2F4, E2F5, E2F6, and E2F7 are 0.12, 0.27, 0.19, and 0.069 respectively, using Kruskal-Walis test.

(C) TGFß suppresses the expression of activating E2Fs, E2F1 and E2F2, in hypoxic HepG2 and TE4 cells. n=3 (biological replicates). Data are represented as mean$\pm$SD; Asterisks represent $p<0.05$ by two-tailed unpaired Student's t-test.

Figure S4. Lung cancers with elevated expression of the 14-gene SASP exhibit increased immune cell infiltration

(A) Volcano plot showing differential expression of cytokines in D-sen and E-sen cells. n=3 biological replicates for each condition. Significantly different cytokines were selected based on Benjamini-Hochberg corrected p-value < 10% and > 2-fold differences in gene expression.

(B) Expression of the 14-gene SASP panel in E-senescent (upper panel) and D-senescent (lower panel) A549 cells. The y-axis represents log2 fold change over untreated A549 cells grown under normoxia (upper panel) or hypoxia (lower panel). n=3 (biological replicates); The 14 cytokines shown in Figure 4A represent those significantly elevated in D-senescent cells compared with E-senescent cells shown in the volcano plot in Figure S4A. They were

selected based on a Benjamini-Hochberg corrected p-value < 10% and > 2-fold differences in gene expression.

(C) Western blot showing that mTOR activity, as measured by phospho-6 and phospho-4EBP1 expression, is suppressed by TGFß (5ng/ml for 15 days) in both normoxic and hypoxic A549 cells compared with untreated cells. pAKT expression in these samples is also shown. GAPDH is provided as control.

(D) Box plots showing that the fraction of myofibroblasts (top) and tumor-derived endothelial cells (bottom; Tumor ECs) (normalized to the number of cancer cells in each sample) are not significantly different across the 14-gene high and 14-gene low lung cancers.

(E) Box plots showing that the fraction of immune cell subtypes shown (normalized to the number of cancer cells in each sample) are significantly higher in lung cancers with a higher fraction of tumor cells expressing high levels of the 14-gene SASP. P values were calculated using two-sample two-sided Wilcoxon test.

Figure S5. The 14-gene high lung cancers exhibit an immune suppressive microenvironment

(A) The 14-gene high lung cancers exhibit an immune suppressive microenvironment. The plots show the ratios of Tregs : exhausted cytotoxic CD8+ T cells and exhausted CD8+T cells : cytotoxic CD8+ T cells (top) and the ratios of NK cells: monocytic macrophages (mo-macs) and cytotoxic CD8+T cells: monocytic macrophages (mo-macs) (bottom) resident within lung cancers harboring a high fraction of 14-gene high cancer cells. $p<0.05$ was calculated using the one-sample two-sided Wilcoxon test applied to (log(x) – log(y)).

(B) Mo-Macs in the 14 cytokine high lung cancers express significantly higher levels of TGFß1. Box plots showing TGFß1 expression in Mo-Macs and myofibroblasts residing in lung cancers with a high and low fraction of tumor cells expressing high and low levels of the 14-gene SASP. P values were calculated using the two-sample two-sided Wilcoxon test.

Figure S6. Lung cancers with high 14-gene SASP expression exhibit adverse clinical outcome

(A) Lung cancers from the publicly available TCGA dataset were characterized based on the expression of the 14-gene SASP. High expression of the 14-gene SASP correlates with adverse clinical outcome by the Cox proportional hazards model applied to relapse-free survival (Log-Rank p = 0.064).

(B) RNA-sequencing data was generated from tumor samples collected from metastatic lung cancer patients prior to initiating immune checkpoint therapy. Cox proportional hazards model applied to the data shows that high expression of the 14-gene SASP in pre-treatment samples trends towards poor progression-free survival (PFS) during the entire follow-up period (mean:316 days; range: 4-1039 days, Log Rank p = 0.065).

Figure S7. Growth characteristics of TGFßR2-KD Lewis lung carcinoma cells

(A) TGFß induces senescence in LLC cells *in vitro*. (Left panel) LLC cells were treated with 5ng/ml TGFß for 15 days and stained for ß-gal activity. Photomicrographs of untreated and TGFß-treated cells stained with ß-gal. Scale bar: 20µm. (Right panel) Bar graph shows the quantification of the percentage of ß-gal positive cells. Mean±SD was calculated from

imaging 4 random fields. Asterisk represents $p<0.05$ by two-tailed unpaired Student's t-test. n=3 biological replicates.

(B) Western blot showing reduced TGFß–induced p-Smad3 levels in TGFßR2-KD LLC1 cells compared with shControl LLC1 cells. Total Smad3 expression is shown as control.

(C) TGFßR2-KD does not impair LLC1 growth *in vitro*. TGFßR2 expression in LLC1 was knocked down using shRNA. Relative growth of shControl and TGFßR2-KD LLC1 *in vitro* is shown. n=3 biological replicates. Each point represents Mean$\pm$SD. n.s: not significant.

(D) The raw intensity histogram of ß-gal stain counts shows that the intensity of the ß-gal signal significantly shifts from strong to weak in the control-to TGFßR2-KD tumors, respectively. n=5 tumors/condition.

(E) p21 staining shows that p21 positive cells significantly decline in shTGFßR2 tumors compared to the control tumors. Left panel shows the photomicrographs of p21 stained shControl and shTGFßR2 tumors. Scale bar: 50µm. Right panel shows quantification of the percentage of p21 positive cells. Mean$\pm$SD was calculated from imaging 5 tumors. Asterisk represents $p<0.0001$ by two-tailed unpaired Student's t-test.

(F) TGFßR2-KD in tumors trends towards a reduction in the ratio of Treg:NK cells compared with shControl tumors. n=5 tumors for each condition. $p=0.055$ calculated by two-tailed unpaired student's t-test.

(G) Staining for Granzyme B, a marker of cytotoxic lymphocytes [51], shows a significant decline in shTGFßR2 tumors compared with control tumors. Scale bar represents 50µm. $p<0.001$ calculated by two-tailed unpaired student's t-test. n=4 tumors/condition.

Figure S1

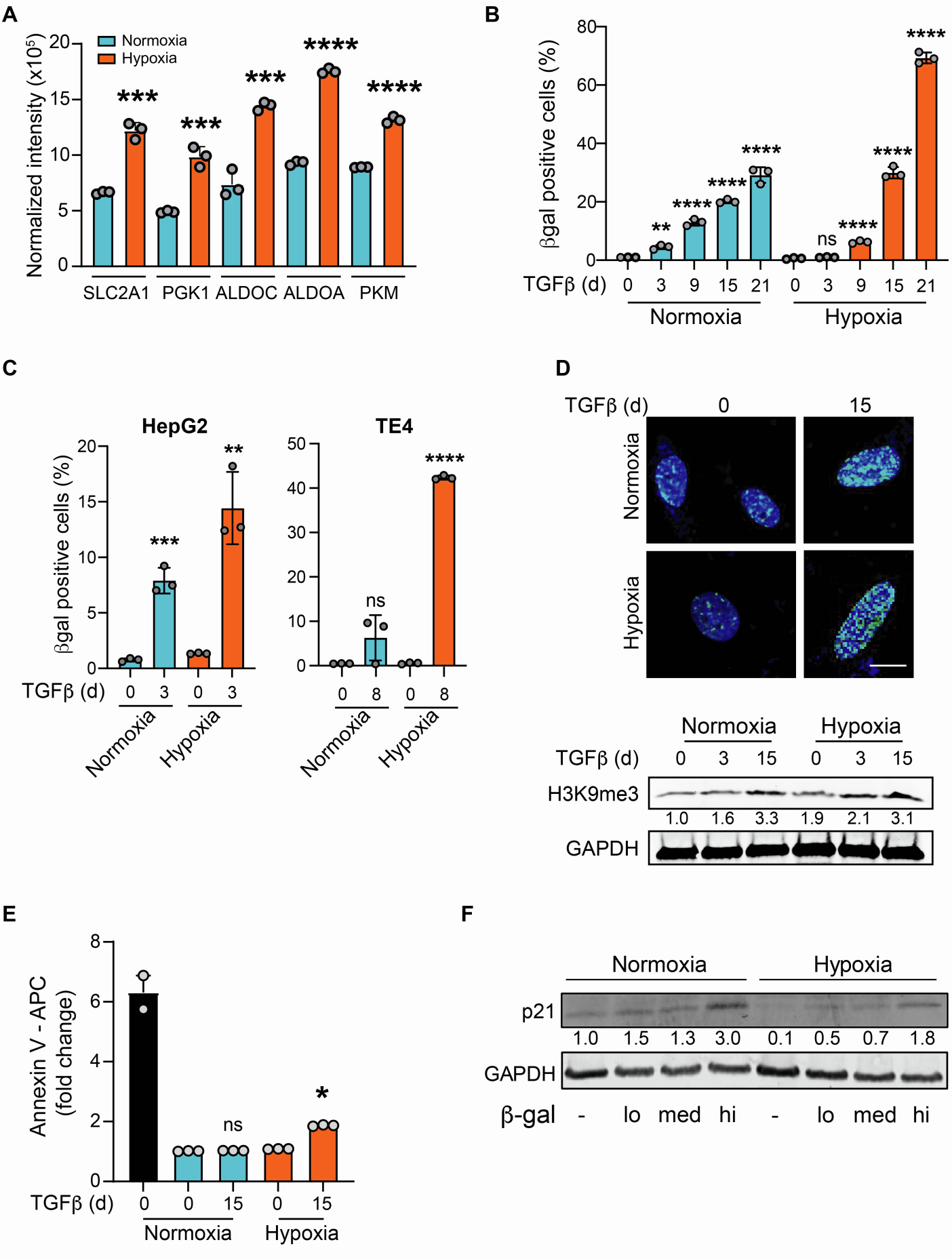
A
Normoxia
Hypoxia
Normalized intensity (x10⁵)
SLC2A1
PGK1
ALDOC
ALDOA
PKM
B
βgal positive cells (%)
TGFβ (d)
Normoxia
Hypoxia
C
HepG2
TE4
βgal positive cells (%)
TGFβ (d)
Normoxia
Hypoxia
D
TGFβ (d)
Normoxia
Hypoxia
H3K9me3
GAPDH
1.0 1.6 3.3 1.9 2.1 3.1
E
Annexin V - APC (fold change)
TGFβ (d)
Normoxia
Hypoxia
F
Normoxia
Hypoxia
p21
GAPDH
1.0 1.5 1.3 3.0 0.1 0.5 0.7 1.8
β-gal - lo med hi - lo med hi

Figure S2

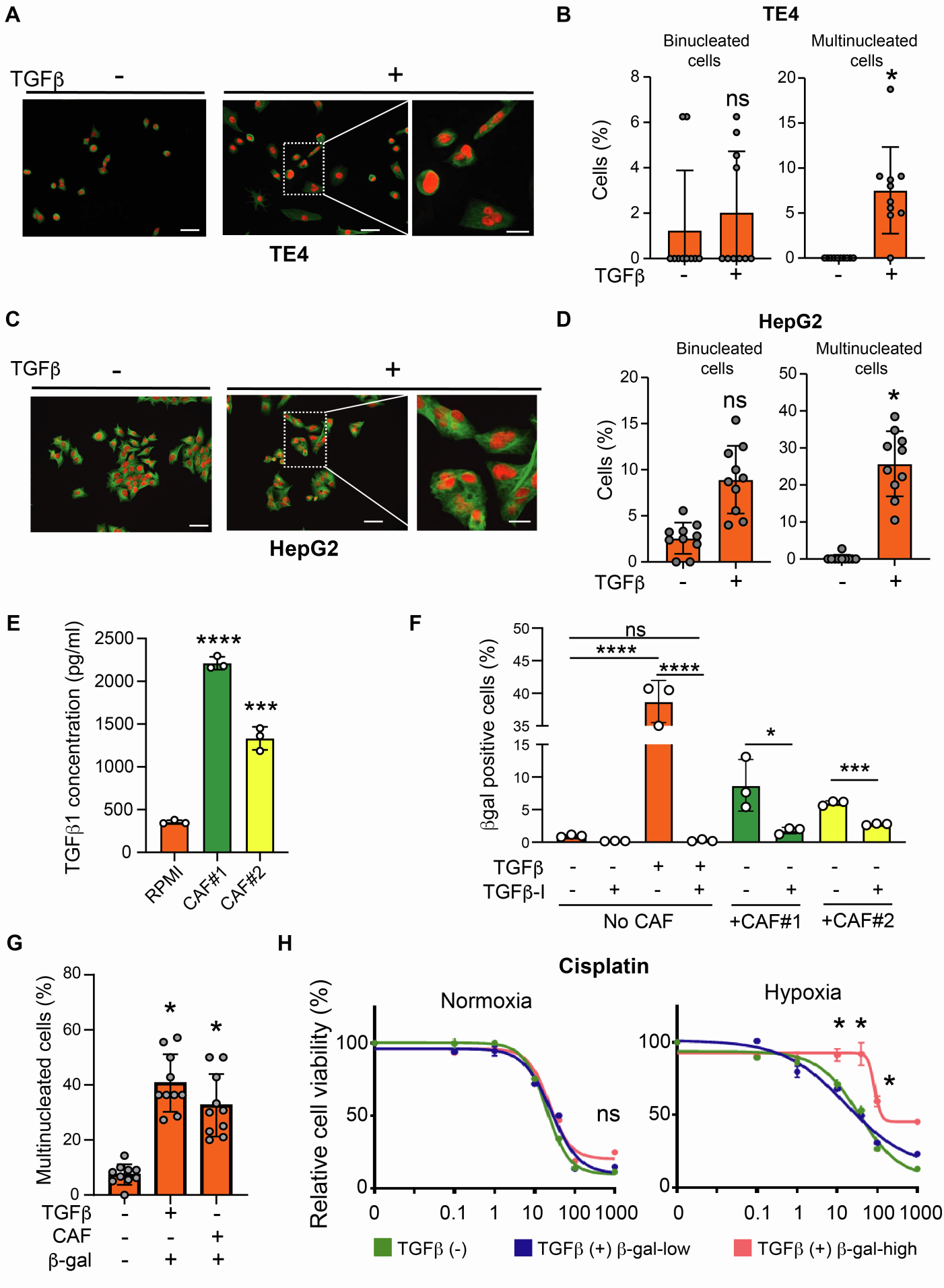
A
TGFβ
-
+
TE4
B
TE4
Binucleated cells
Multinucleated cells
Cells (%)
ns
*
TGFβ
C
HepG2
D
HepG2
E
TGFβ1 concentration (pg/ml)
****
***
RPMI
CAF#1
CAF#2
F
βgal positive cells (%)
ns
****
*
***
TGFβ
TGFβ-I
No CAF
+CAF#1
+CAF#2
G
Multinucleated cells (%)
TGFβ
CAF
β-gal
H
Cisplatin
Normoxia
Hypoxia
Relative cell viability (%)
TGFβ (-)
TGFβ (+) β-gal-low
TGFβ (+) β-gal-high

Figure S3

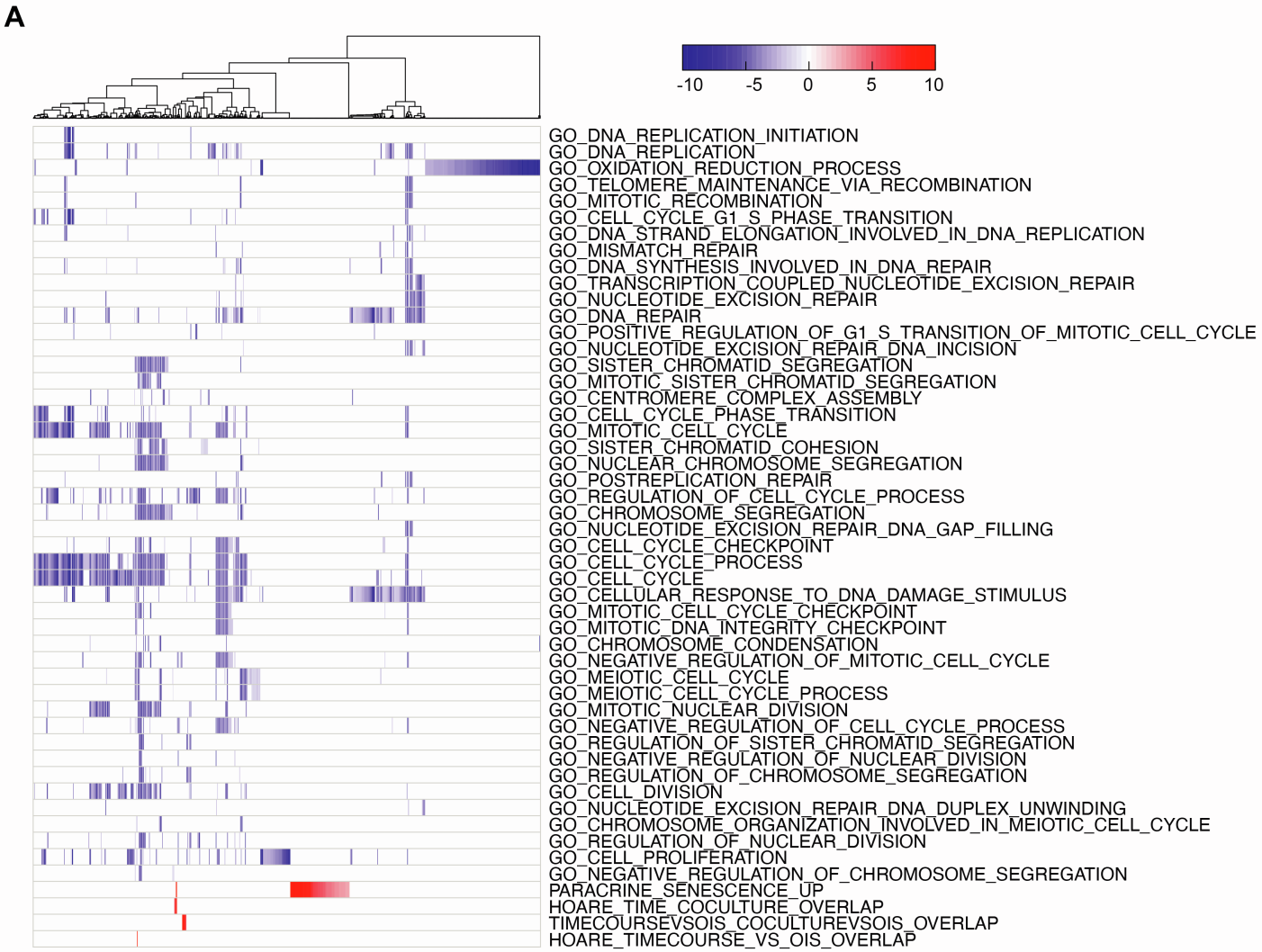
A
-10
-5
0
5
10
GO_DNA_REPLICATION_INITIATION
GO_DNA_REPLICATION
GO_OXIDATION_REDUCTION_PROCESS
GO_TELOMERE_MAINTENANCE_VIA_RECOMBINATION
GO_MITOTIC_RECOMBINATION
GO_CELL_CYCLE_G1_S_PHASE_TRANSITION
GO_DNA_STRAND_ELONGATION_INVOLVED_IN_DNA_REPLICATION
GO_MISMATCH_REPAIR
GO_DNA_SYNTHESIS_INVOLVED_IN_DNA_REPAIR
GO_TRANSCRIPTION_COUPLED_NUCLEOTIDE_EXCISION_REPAIR
GO_NUCLEOTIDE_EXCISION_REPAIR
GO_DNA_REPAIR
GO_POSITIVE_REGULATION_OF_G1_S_TRANSITION_OF_MITOTIC_CELL_CYCLE
GO_NUCLEOTIDE_EXCISION_REPAIR_DNA_INCISION
GO_SISTER_CHROMATID_SEGREGATION
GO_MITOTIC_SISTER_CHROMATID_SEGREGATION
GO_CENTROMERE_COMPLEX_ASSEMBLY
GO_CELL_CYCLE_PHASE_TRANSITION
GO_MITOTIC_CELL_CYCLE
GO_SISTER_CHROMATID_COHESION
GO_NUCLEAR_CHROMOSOME_SEGREGATION
GO_POSTREPLICATION_REPAIR
GO_REGULATION_OF_CELL_CYCLE_PROCESS
GO_CHROMOSOME_SEGREGATION
GO_NUCLEOTIDE_EXCISION_REPAIR_DNA_GAP_FILLING
GO_CELL_CYCLE_CHECKPOINT
GO_CELL_CYCLE_PROCESS
GO_CELL_CYCLE
GO_CELLULAR_RESPONSE_TO_DNA_DAMAGE_STIMULUS
GO_MITOTIC_CELL_CYCLE_CHECKPOINT
GO_MITOTIC_DNA_INTEGRITY_CHECKPOINT
GO_CHROMOSOME_CONDENSATION
GO_NEGATIVE_REGULATION_OF_MITOTIC_CELL_CYCLE
GO_MEIOTIC_CELL_CYCLE
GO_MEIOTIC_CELL_CYCLE_PROCESS
GO_MITOTIC_NUCLEAR_DIVISION
GO_NEGATIVE_REGULATION_OF_CELL_CYCLE_PROCESS
GO_REGULATION_OF_SISTER_CHROMATID_SEGREGATION
GO_NEGATIVE_REGULATION_OF_NUCLEAR_DIVISION
GO_REGULATION_OF_CHROMOSOME_SEGREGATION
GO_CELL_DIVISION
GO_NUCLEOTIDE_EXCISION_REPAIR_DNA_DUPLEX_UNWINDING
GO_CHROMOSOME_ORGANIZATION_INVOLVED_IN_MEIOTIC_CELL_CYCLE
GO_REGULATION_OF_NUCLEAR_DIVISION
GO_CELL_PROLIFERATION
GO_NEGATIVE_REGULATION_OF_CHROMOSOME_SEGREGATION
PARACRINE_SENESCENCE_UP
HOARE_TIME_COCULTURE_OVERLAP
TIMECOURSEVSOIS_COCULTUREVSOIS_OVERLAP
HOARE_TIMECOURSE_VS_OIS_OVERLAP

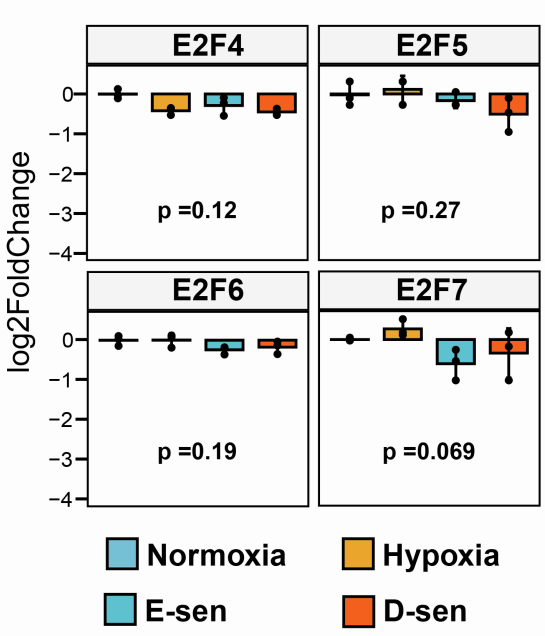
B
E2F4
E2F5
E2F6
E2F7
log2FoldChange
0
−1
−2
−3
−4
p =0.12
p =0.27
p =0.19
p =0.069
Normoxia
Hypoxia
E-sen
D-sen

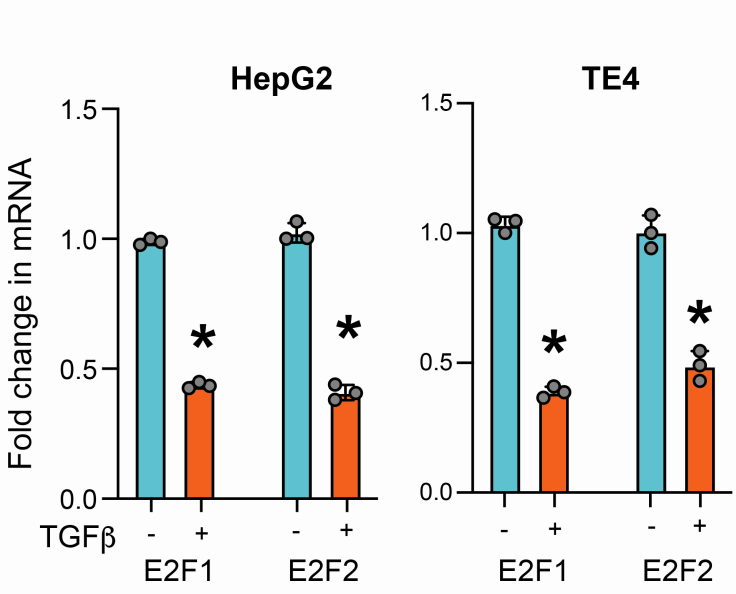
C
HepG2
TE4
Fold change in mRNA
1.5
1.0
0.5
0.0
*
TGFβ
-
+
E2F1
E2F2

Figure S4

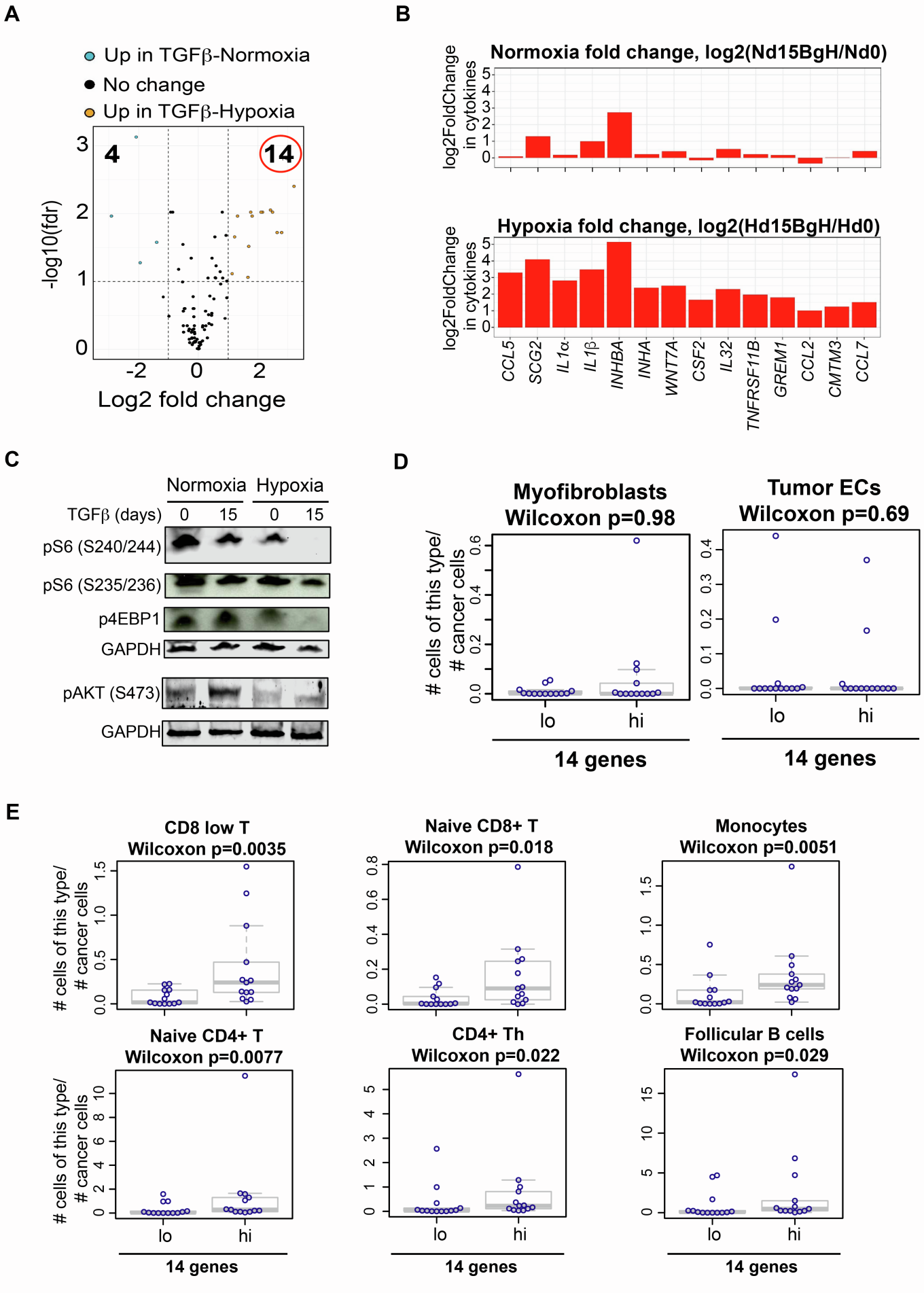
A
Up in TGFβ-Normoxia
No change
Up in TGFβ-Hypoxia
4
14
-log10(fdr)
Log2 fold change
B
Normoxia fold change, log2(Nd15BgH/Nd0)
log2FoldChange in cytokines
Hypoxia fold change, log2(Hd15BgH/Hd0)
CCL5
SCG2
IL1α
IL1β
INHBA
INHA
WNT7A
CSF2
IL32
TNFRSF11B
GREM1
CCL2
CMTM3
CCL7
C
Normoxia
Hypoxia
TGFβ (days)
0
15
0
15
pS6 (S240/244)
pS6 (S235/236)
p4EBP1
GAPDH
pAKT (S473)
GAPDH
D
Myofibroblasts
Wilcoxon p=0.98
Tumor ECs
Wilcoxon p=0.69
cells of this type/
cancer cells
lo
hi
14 genes
E
CD8 low T
Wilcoxon p=0.0035
Naive CD8+ T
Wilcoxon p=0.018
Monocytes
Wilcoxon p=0.0051
Naive CD4+ T
Wilcoxon p=0.0077
CD4+ Th
Wilcoxon p=0.022
Follicular B cells
Wilcoxon p=0.029

Figure S5

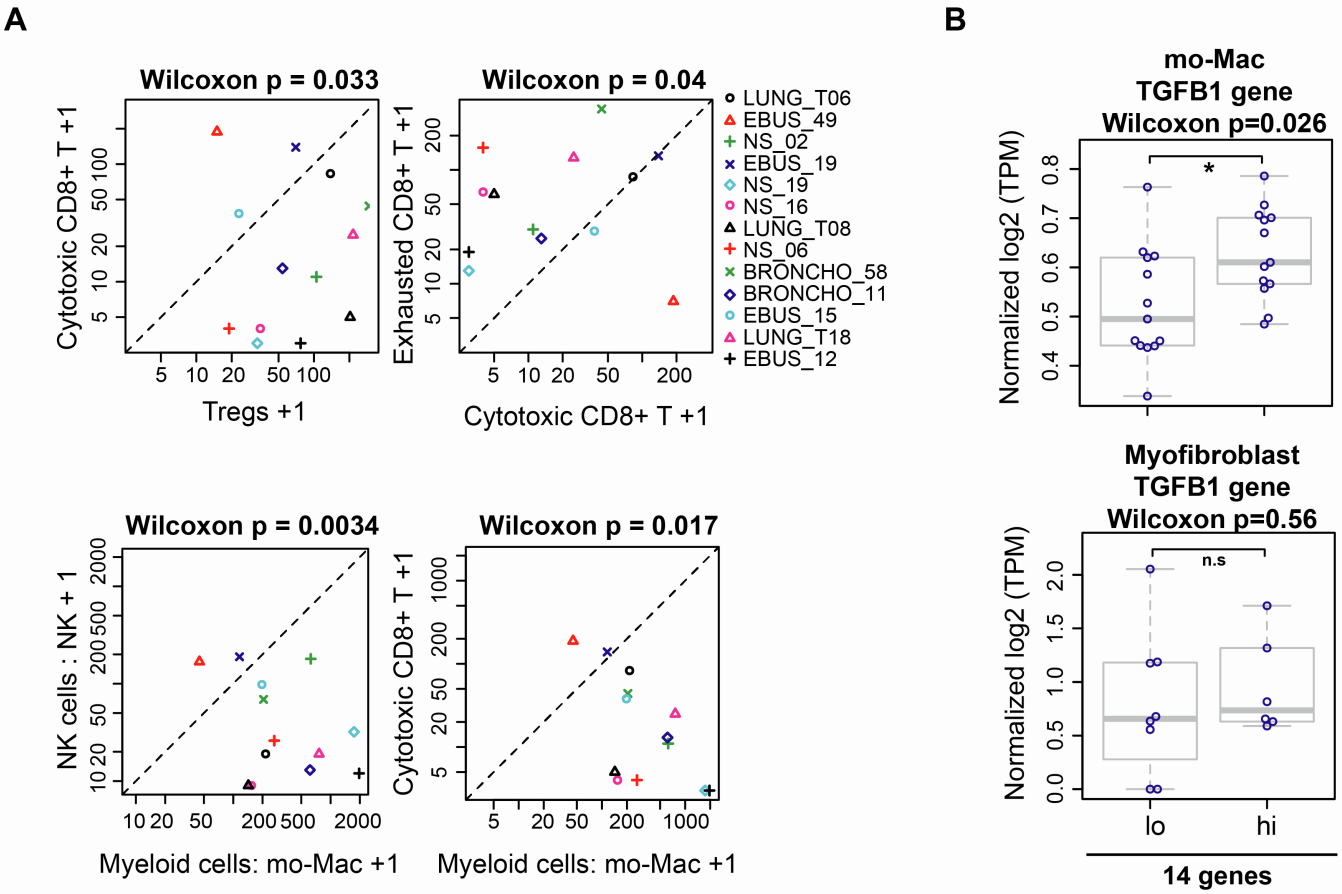
A
Wilcoxon p = 0.033
Cytotoxic CD8+ T +1
Tregs +1
Wilcoxon p = 0.04
Exhausted CD8+ T +1
Cytotoxic CD8+ T +1
LUNG_T06
EBUS_49
NS_02
EBUS_19
NS_19
NS_16
LUNG_T08
NS_06
BRONCHO_58
BRONCHO_11
EBUS_15
LUNG_T18
EBUS_12
Wilcoxon p = 0.0034
NK cells : NK + 1
Myeloid cells: mo-Mac +1
Wilcoxon p = 0.017
Cytotoxic CD8+ T +1
Myeloid cells: mo-Mac +1
B
mo-Mac
TGFB1 gene
Wilcoxon p=0.026
Normalized log2 (TPM)
*
Myofibroblast
TGFB1 gene
Wilcoxon p=0.56
Normalized log2 (TPM)
n.s
lo
hi
14 genes

Figure S6

A

LUAD-TCGA

Relapse-Free Survival
(log-rank p=0.063)

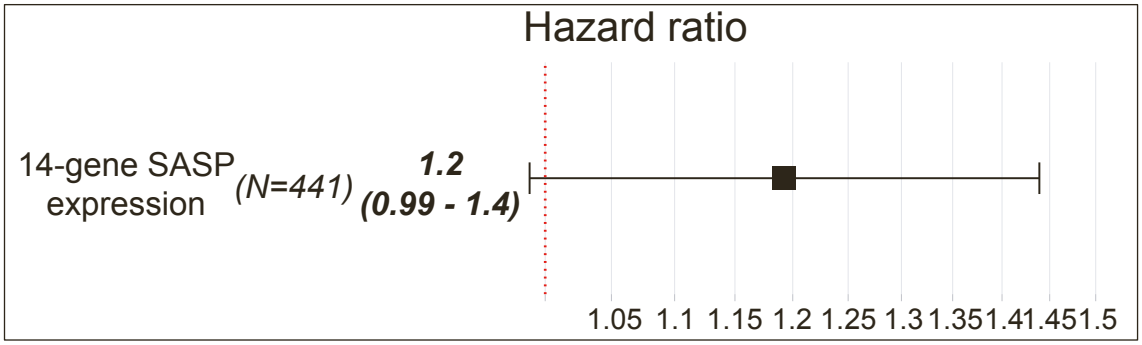

 # Events: 151; Global p-value (Log-Rank): 0.0635
AIC: 1581.98; Concordance Index: 0.56

B

NSCLC immune checkpoint inhibitor therapy

Progression-free Survival
(mean:316 days; range 4-1039 days)
(log-rank p=0.065)

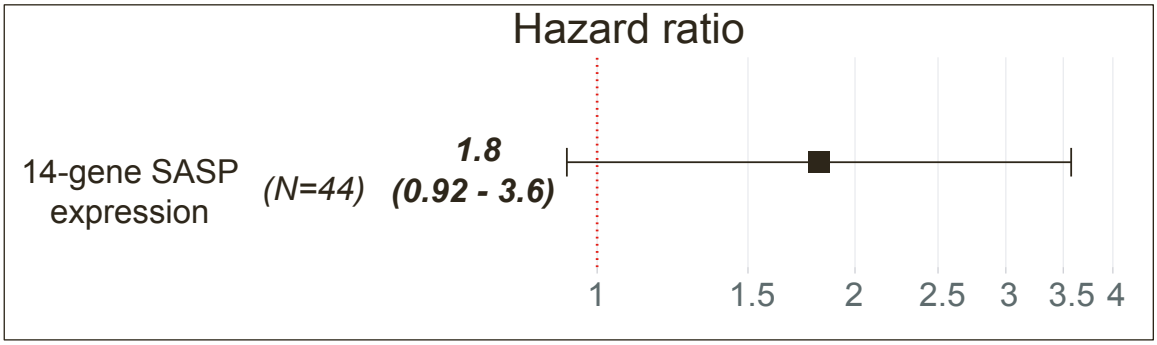

 # Events: 26; Global p-value (Log-Rank): 0.065442
AIC: 159.94; Concordance Index: 0.61

Figure S7

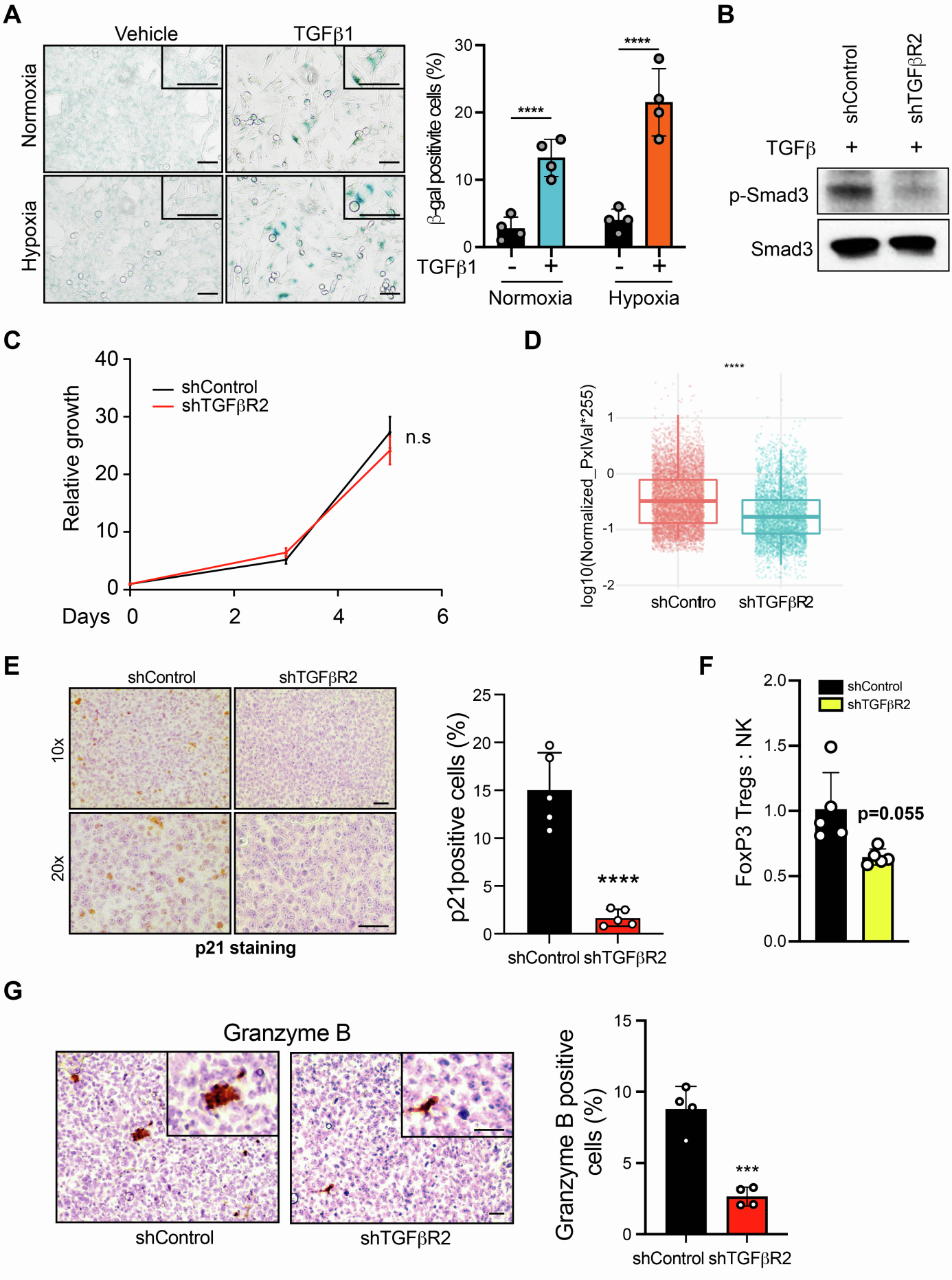
A
Vehicle
TGFβ1
Normoxia
Hypoxia
β-gal positivite cells (%)
30
20
10
0
****
****
TGFβ1
-
+
-
+
Normoxia
Hypoxia
B
shControl
shTGFβR2
TGFβ
+
+
p-Smad3
Smad3
C
Relative growth
40
30
20
10
0
shControl
shTGFβR2
n.s
Days
0
2
4
6
D
****
log10(Normalized_PxlVal*255)
1
0
-1
-2
shContro
shTGFβR2
E
shControl
shTGFβR2
10x
20x
p21 staining
p21positive cells (%)
25
20
15
10
5
0
****
shControl
shTGFβR2
F
FoxP3 Tregs : NK
2.0
1.5
1.0
0.5
0.0
shControl
shTGFβR2
p=0.055
G
Granzyme B
shControl
shTGFβR2
Granzyme B positive cells (%)
15
10
5
0
***
shControl
shTGFβR2